Effects of Pulse Accumulation on Femtosecond-Laser-Induced Periodic Surface Structures in Si and SiC

Kohei Chigusa[1], Kaito Fukuda[1], Tatsuya Okada[1], and Takuro Tomita[*1]

[1]*Graduate School of Science and Technology for Innovation, Tokushima University, Japan*
[*]*Corresponding author's e-mail: tomita@tokushima-u.ac.jp*

To investigate the effects of pulse accumulation in femtosecond laser processing, we developed an *in-situ* observation system by incorporating an optical window into a scanning electron microscope (SEM). This enabled *in-situ*, pulse-by-pulse monitoring of evolution of laser-induced periodic surface structures (LIPSS) on single-crystal silicon (Si) and silicon carbide (SiC) under identical irradiation conditions. On Si, LIPSS initially appeared with a period comparable to the laser wavelength and progressively increased in both period and groove width with successive pulses, indicating a positive feedback mechanism. In contrast, SiC exhibited stable LIPSS with a constant period of 160–200 nm throughout the irradiation. Additionally, focused ion beam (FIB) pretreatment on Si surfaces enhanced local electric fields, resulting in groove widening and preferential LIPSS formation near the modified regions. These findings support the hypothesis that initial surface morphology plays a critical role in modulating ablation dynamics through local field enhancement.
DOI: 10.2961/jlmn.2025.02.2012
Keywords: laser-induced periodic surface structures (LIPSS), femtosecond laser, scanning electron microscopy (SEM), *in-situ* observation, FIB pre-treatment

1. Introduction

Femtosecond laser-induced surface ablation has garnered significant attention due to its relevance in both fundamental studies and a range of industrial applications. Among various laser-material interaction phenomena, the formation of nanostructures—particularly laser-induced periodic surface structures (LIPSS)—has attracted considerable interest because of their potential in surface micro- and nanofabrication [1–7]. In this study, we detail the experimental setup and analyze the pulse-accumulated progression of surface ablation induced by femtosecond laser irradiation.

Understanding the mechanisms underlying laser ablation requires consideration of two primary aspects. First, single-pulse ablation dynamics can be examined using time-resolved imaging techniques [8–11]. Second, the cumulative effects of sequential laser pulses significantly influence LIPSS formation through either positive or negative feedback processes. While single-pulse dynamics have been extensively studied, investigations into pulse-by-pulse structural evolution remain relatively limited.

LIPSS typically range from tens to hundreds of nanometers, which exceeds the resolution limits of conventional optical microscopy. In contrast, scanning electron microscopy (SEM) offers sufficient spatial resolution to visualize these fine structures. However, acquiring SEM images after each individual pulse poses substantial technical challenges. Moreover, the inherently non-reproducible nature of laser ablation introduces variability even under nominally identical conditions. This variability stems from the high sensitivity of laser-material interactions to initial surface conditions [12], making it nearly impossible to prepare perfectly identical samples for repeated experiments. These challenges underscore the need for high-resolution techniques capable of monitoring the pulse-by-pulse evolution of surface structures.

To overcome these limitations, we developed an *in-situ* observation system by integrating an optical window into an SEM, enabling femtosecond laser irradiation to be conducted directly within the sample chamber. This system allowed real-time tracking of ablation dynamics by alternating between laser exposure and SEM imaging without repositioning the sample. In this study, we present the technical details of this system and investigate the ablation behavior of silicon (Si) and silicon carbide (SiC) single crystals under identical irradiation conditions.

2. Experimental

The femtosecond laser source used in this study was a Ti:sapphire regenerative amplifier (Spectra-Physics, Solstice) based on a chirped pulse amplification (CPA) system, operating at a central wavelength of 800 nm. It produced pulses with a duration of 130 fs at a repetition rate of 1 kHz. A schematic of the experimental setup is shown in Figure 1.

The laser beam was initially directed through a half-wave plate, a mechanical shutter, and a polarizing beam splitter (PBS). The laser fluence was adjusted by rotating the half-wave plate to control the transmission ratio through the PBS. The beam was then focused onto the sample surface using a plano-convex lens with a focal length of 400 mm, passing through a custom-designed optical window integrated into the SEM chamber (see Fig. 1).

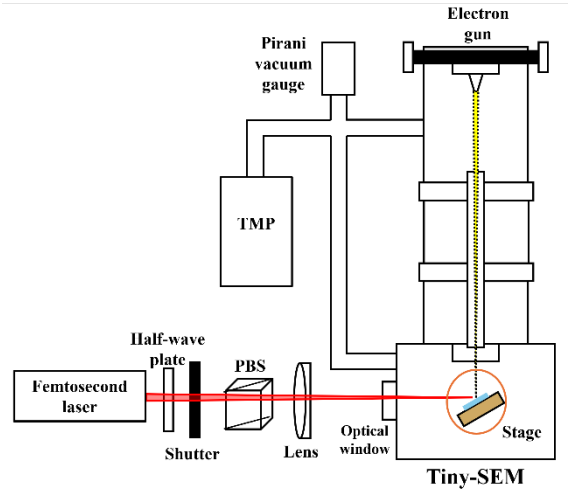

Fig.1 An optical window was installed into the Tiny-SEM chamber to enable the introduction of femtosecond laser pulses. Tilting the sample stage by 30° resulted in a laser incidence angle of 60° with respect to the surface normal.

The samples used in this experiment were single-crystal silicon (Si (100)) and silicon carbide. The substrate used in this study is an n-type 4H-SiC wafer doped with nitrogen, with a doping concentration of 1×10^{15} cm^{-3}. The surface orientation is 4° off-axis from the (0001) basal plane toward the <11-20> crystallographic direction. The laser fluence was determined using the Liu's method [13], yielding 1.44 J/cm² for Si, 1.65 J/cm² for SiC and 1.16 J/cm² for the FIB-marked Si. In this study, the spot size was not measured directly using a CMOS or CCD camera. Instead, the spot radius was estimated using Liu's method, based on the radius of the ablation crater produced by 1000 pulse irradiation at each location. A plano-convex lens with a focal length of 400 mm was used to focus the femtosecond laser onto the sample surface.

The spot radii estimated using this method were 39.7 µm for the Si substrate, 46.0 µm for the SiC substrate, and 39.3 µm for the FIB-marked Si region. An example of Liu's method result for Si is shown in Figure 2. The same method was applied to SiC and the FIB-marked Si as well.

Although direct optical beam profiling was not conducted, the laser beam was assumed to exhibit a Gaussian spatial profile based on the specifications and typical performance characteristics of the laser system used.

Each sample was mounted at a tilt angle of 30° with respect to the incident beam. In this study, the laser was incident at an angle of 60° with respect to the sample surface normal, with the polarization set to s-polarization. When silicon surfaces are irradiated with multiple pulses of 800 nm, 100 fs laser light, the ablation threshold fluence is reported to be F_{th} = 0.2 J/cm² [14] or F_{th} = 0.12 J/cm² [15] under normal incidence. In the present study, however, material modification was observed only at fluences exceeding these threshold values. Under such oblique incidence and polarization conditions, the electric field component of the laser becomes parallel to the surface, reducing the absorption efficiency. As a result, a higher fluence is required to induce ablation. A similar trend has been reported for metals, where the ablation threshold increases by approximately a factor of two under s-polarized oblique incidence [16]. The elevated

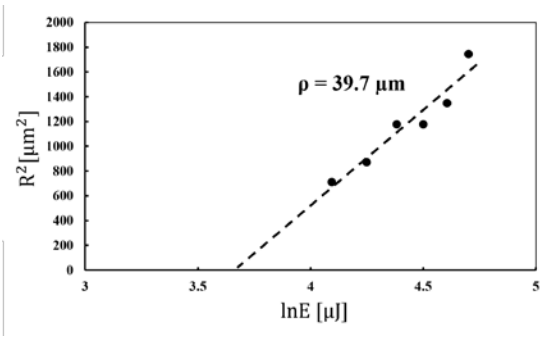

Fig.2 Plot of the squared radius of ablation craters formed on the Si substrate after 1000-pulse irradiation as a function of the natural logarithm of the laser fluence (ln E). A linear fit based on the Liu's method was applied to estimate the laser spot size and the ablation threshold fluence.

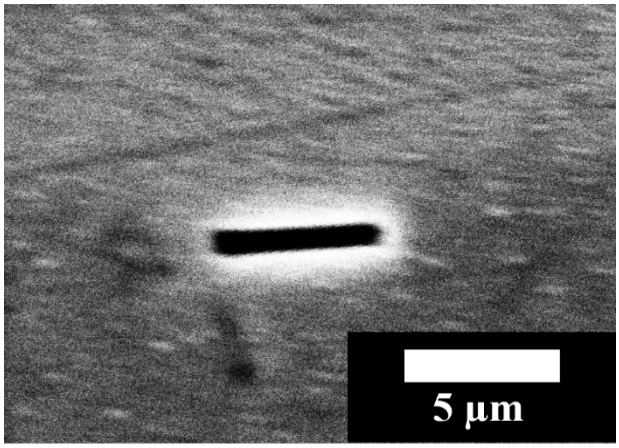

Fig.3 Initial structuring was carried out using focused ion beam (FIB). The FIB mark measures 6 µm in length, 1 µm in width and 1 µm in depth.

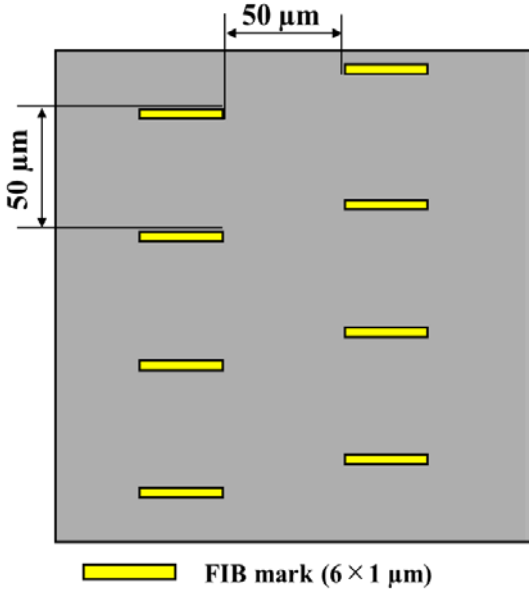

Fig.4 Top-view of the periodic arrangement of FIB marks on a silicon substrate. Each rectangular mark has a length of 6 µm, width of 1 µm, and depth of 1µm, and they are spaced at 50 µm intervals. This layout was designed to study the influence of laser irradiation at various positions relative to the beam center.

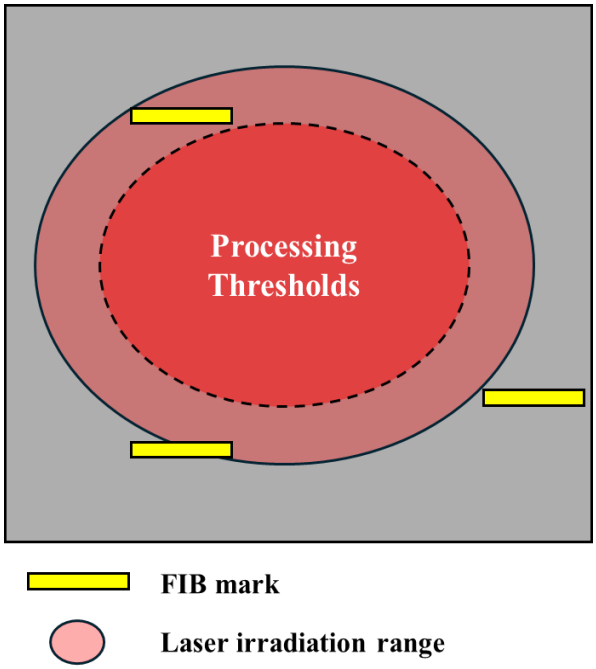

Fig.5 Magnified schematic of the laser irradiation spot. A femtosecond laser beam (indicated in red) is irradiated over an area that includes multiple FIB marks (in yellow) in its peripheral region. The study focuses on processing behavior in regions where the laser fluence is below the ablation threshold.

thresholds observed for Si and SiC in this study are considered to arise from the same physical mechanism. A TinySEM (model 1710, TECHNEX) was used for imaging, and the chamber vacuum was maintained at 3×10^{-2} Pa. SEM observations were performed using a tabletop SEM operated at a relatively low accelerating voltage of approximately 13 kV. Under these conditions, no charging artifacts were observed during imaging, and conductive coating was not required.

Laser irradiation was performed in separate shots. One laser shot contained 125 pulses, controlled by setting the mechanical shutter to remain open for 1/8 of a second. The total accumulated number of pulses was 1000 for Si and 6000 for SiC. SEM images were obtained after each shot to observe the progression of surface modifications.

To analyze the periodicity of the LIPSS, fast Fourier transform (FFT) analysis was applied to the SEM images. The FFT decomposed the spatial frequency components and quantified their amplitude intensities. The LIPSS period was calculated as the inverse of the dominant spatial frequency. However, due to spectral noise, it was often difficult to directly extract accurate periodicities from the FFT spectra. To address this, moment analysis was employed to compute the weighted average of the spatial frequency distribution, and the mean LIPSS period was then obtained as the inverse of the spectral center of gravity.

To investigate whether LIPSS can form under laser fluence conditions below the ablation threshold, we performed a localized surface modification on single-crystalline silicon samples using a focused ion beam (FIB) system. As illustrated in Figure 3, rectangular marks with dimensions of 1 μm (width) × 6 μm (length) × 1 μm (depth) were fabricated on the surface. These marks were aligned linearly with a spacing of 50 μm, as shown in Figure 4.

After the FIB marking, the sample was irradiated with femtosecond laser pulses under sub-threshold fluence conditions—that is, below the ablation or clear surface modification threshold for unstructured Si. The laser spot was aligned so that the peripheral region of each irradiated area overlapped on the FIB marks (Figure 5). The purpose of this configuration was to evaluate whether localized electric field enhancement around the FIB-induced marks could facilitate LIPSS formation even under fluence conditions insufficient to induce structural change on a flat surface.

3. Results and discussion

Silicon (Si) and silicon carbide (SiC) were selected as target materials for this study. Si was chosen due to its widespread industrial application and the availability of extensive research data on LIPSS formation. SiC was selected for its growing relevance in power electronics, as well as its high durability, thermal conductivity, and superior capacity to form finer periodic structures compared to Si.

Figure 6 shows *in-situ* SEM images of the Si surface after femtosecond laser irradiation. The experiments shown in Figures 6 and 9 were conducted using Si and SiC samples that were not subjected to FIB processing. The *in-situ* approach enabled consistent imaging of the same location after each laser pulse sequence, allowing detailed observation of gradual structural changes, including groove widening prior

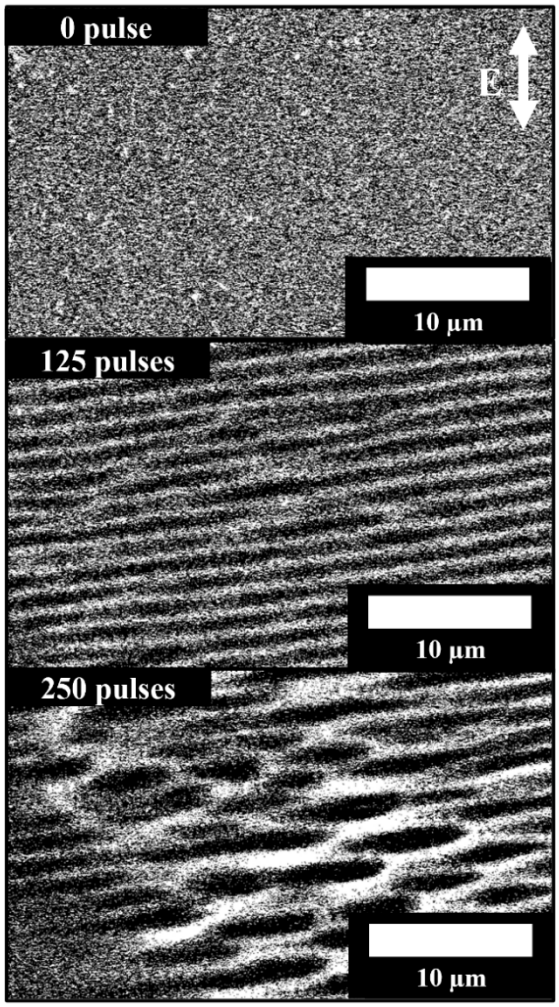

Fig.6 *In-situ* SEM images of Si irradiated with a femtosecond laser at a fluence of 1.44 J/cm², recorded every 125 pulses.

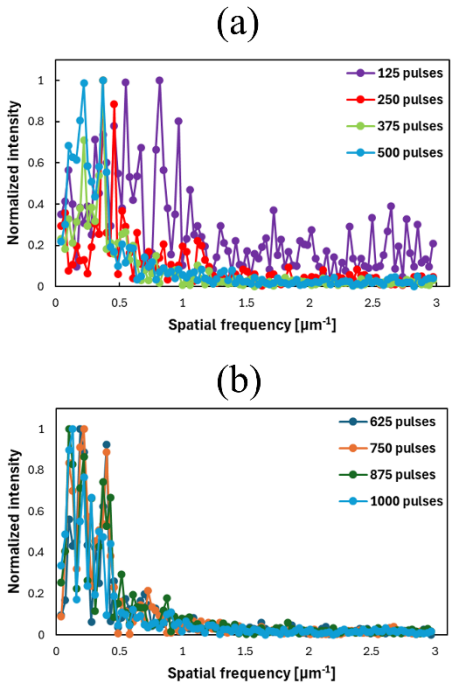

Fig.7 FFT spectra obtained from SEM images of the Si surface irradiated with 125 to 1000 laser pulses, showing changes in the periodic peaks corresponding to LIPSS formation.
(a) FFT spectra for 125 to 500 pulses.
(b) FFT spectra for 625 to 1000 pulses.

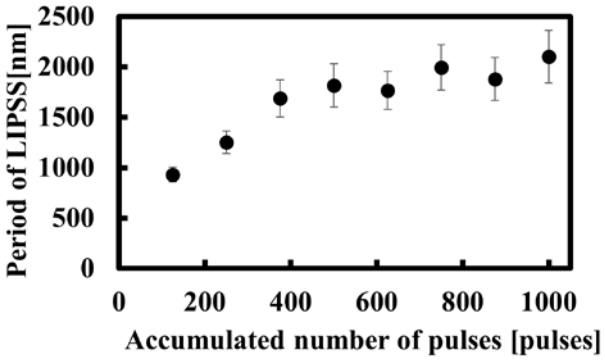

Fig.8 The effects of accumulated laser pulses on LIPSS on Si surface: FFT analysis of *in-situ* SEM images irradiated with a laser fluence of 1.44 J/cm², conducted every 125 pulses up to 1000 pulses, along with corresponding moment analysis results.

to the appearance of well-defined LIPSS. At 0 pulses, the surface appeared smooth and undamaged. After 125 pulses, periodic structures began to emerge, and after 250 pulses, groove widening was clearly visible. To quantitatively evaluate the evolution of LIPSS, FFT was applied to SEM images obtained under different pulse number conditions. Figure 7 presents the FFT spectra for Si corresponding to pulse counts ranging from 125 to 1000. To highlight the periodic features associated with LIPSS, low-frequency components not related to the structures were removed from the spectra.

In several cases, the main spectral peak was unclear, making direct peak identification unreliable for determining the LIPSS period. To address this, a first-order moment analysis was performed on the spatial frequency distribution derived from each FFT spectrum. The centroid frequency calculated from the first-order moment was used to determine the average period of the LIPSS. Furthermore, the variance derived from the second-order moment was used as a measure of dispersion and represented as error bars.

The mathematical definitions of the first and second-order moments used in this study are as follows:

$$M_1 = \frac{1}{M_0}\int E \times I(E)dE, \quad (1)$$

$$M_2 = \frac{1}{M_0}\int (E - M_1)^2 \times I(E)dE, \quad (2)$$

where M_0 is the total integrated intensity, E is the spatial frequency, I(E) is the spectral intensity at frequency E, M_1 is the centroid frequency, and M_2 is the variance. This moment-based approach enabled reliable quantification of the LIPSS period, even in spectra with substantial noise. The results for the Si samples are summarized in Figure 8. It should be noted that the calculated values reflect the spread of the spatial frequency distribution within the observed region and do not represent the average or variance of the LIPSS period

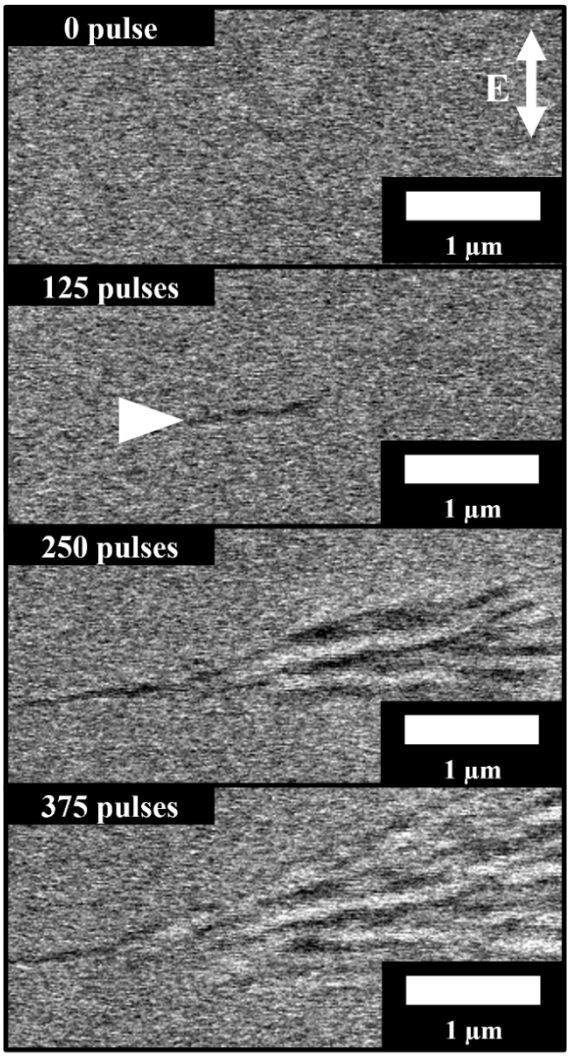

Fig.9 *In-situ* SEM imaging of SiC irradiated with a laser fluence of 1.65 J/cm², captured at intervals of every 125 pulses. Linear structures began to develop after 125 pulses as shown by the white arrowhead.

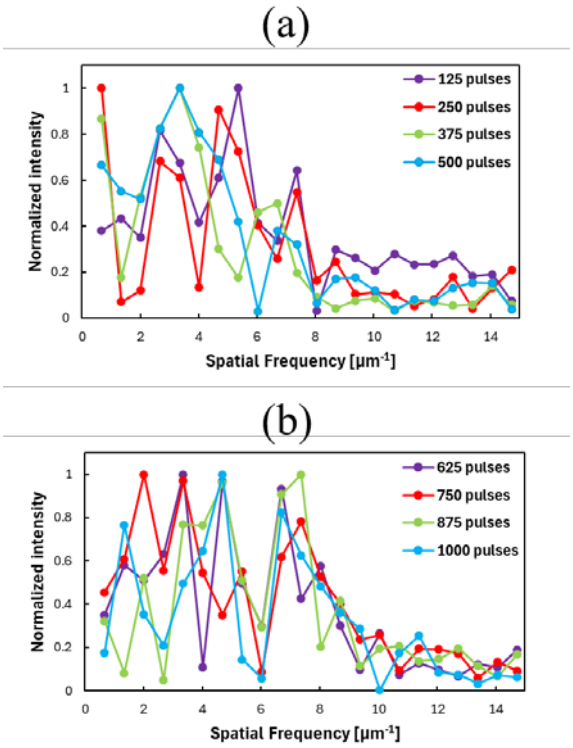

Fig.10 FFT spectra obtained from SEM images of the SiC surface irradiated with 125 to 1000 laser pulses, showing changes in the periodic peaks corresponding to LIPSS formation.
(a) FFT spectra for 125 to 500 pulses.
(b) FFT spectra for 625 to 1000 pulses.

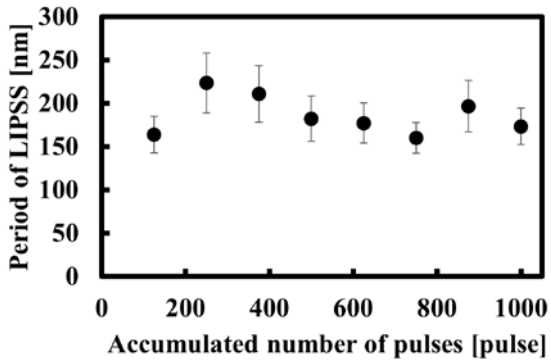

Fig.11 The dependence of accumulated laser pulses on LIPSS on SiC surface: FFT analysis of *in-situ* SEM images of SiC irradiated with a laser fluence of 1.65 J/cm², acquired every 125 pulses from 0 to 1000 pulses, along with corresponding moment analysis results.

across different surface locations. The results indicate that the LIPSS period on Si increases with pulse accumulation.

Figure 9 displays an *in-situ* SEM image of the SiC surface after laser shots. The pristine surface (0 pulses) was smooth, and linear structures began to appear after 125 pulses as indicate by the white arrowhead. After 250 pulses, these evolved into more complex, branched structures. As with the Si sample, FFT and moment analyses were performed, and the results are shown in Figures 10 and 11. In contrast to Si, the period of LIPSS on SiC remained nearly constant throughout irradiation, indicating higher structural stability and lower sensitivity to cumulative pulse effects.

The comparison of SEM images of Si and SiC reveals distinct differences in groove width evolution. In Si, groove width increases significantly with the number of laser pulses, whereas in SiC, it remains nearly constant. The groove widening observed in Si is likely attributable to the enhancement of local electric fields resulting from repeated irradiation of preexisting LIPSS. In the present *in-situ* observation system, multiple laser pulses irradiate the same location, which means that the initial surface structure influences the local electric field distribution during subsequent pulses. The preformed LIPSS are presumed to concentrate the electric field locally, thereby triggering a positive feedback mechanism. Under *s*-polarized light, surface plasmon polariton (SPP) excitation is suppressed [17], and thus the interference between scattered light and surface roughness dominates the formation of LIPSS. As the surface structure evolves with increasing pulse number, enhanced scattering and optical interference promote the development of longer-period features, leading to a gradual increase in LIPSS periodicity on Si.

In contrast, the LIPSS period on SiC remains nearly constant. This stability is attributed to the high thermal conductivity and strong resistance to oxidation and heat in SiC, which together suppress changes in both structural and optical properties during irradiation. Furthermore, the semi-transparency of SiC allows partial laser energy transmission into the bulk, thereby reducing surface absorption. These characteristics inhibit the formation of a positive feedback loop, resulting in more stable surface patterns with consistent periodicity.

In general, LIPSS tend to form in a direction perpendicular to the electric field vector of the incident laser polarization, which is s-polarized in this study. However, as seen in Figures. 6, 9, and 12, the orientation of the LIPSS grooves appears slightly tilted from the expected direction in some cases. This tilt may be due to a minor misalignment in the optical setup used in the experiment. Since precise spatial overlap of the femtosecond laser beam and the SEM electron beam was required, high-precision adjustment of the optical components was necessary. Slight angular deviations or mechanical strain in elements such as mirrors or beam splitters may have caused the polarization plane to rotate slightly from its intended orientation. Consequently, the actual direction of the electric field at the sample surface may have deviated slightly, resulting in the observed tilt of the LIPSS grooves.

The classification of the LIPSS observed in this study was based on their spatial period. In general, LIPSS are categorized as low-spatial-frequency LIPSS (LSFL) when their period is approximately equal to or greater than the laser wavelength (λ), and as high-spatial-frequency LIPSS (HSFL) when their period is shorter than λ/2. In this study, the laser wavelength used was 800 nm. The LIPSS formed on the Si substrate exhibited a period of approximately 800 nm, and were therefore classified as LSFL. In contrast, the LIPSS formed on the SiC substrate had a period of approximately 200 nm, and were classified as HSFL.

To examine whether LIPSS can form under laser fluence conditions below the ablation threshold, localized marks were fabricated on the silicon surface using a focused ion beam (FIB), as illustrated in Figure 3. Each FIB mark measured 1 μm in width, 6 μm in length, and 1 μm in depth. These

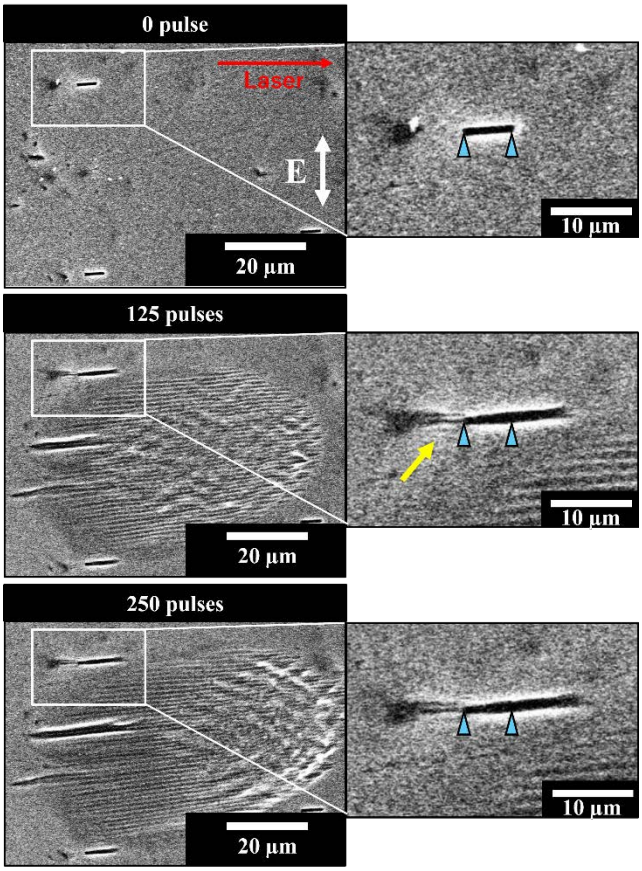

Fig.12 SEM images near the FIB marks before (0 pulse) and after laser irradiation (125, 250 pulses). Laser irradiation was performed near the FIB marks so that they were irradiated below the processing threshold. The laser fluence was set to 1.16 J/cm². The left images show wide-area SEM views, while the right images are magnified views around the FIB mark. This result was obtained from the experiment performed on the Si sample.

marks were arrayed at intervals of 50 μm, as shown in Figure 4. The laser was irradiated so that only the peripheral region of a laser spot, i.e., the sub-threshold region (below the processing threshold) overlapped on the FIB marks (Figure 5). Since local enhancements in electric field around the FIB marks may facilitate material modification even under sub-threshold conditions, this possibility was systematically investigated. As shown in Figure 12, the FIB marks were clearly visible before laser irradiation. In the peripheral region of the laser spot, morphological changes were observed only around the FIB marks (125 pulses, 250 pulses). The FIB marks showed an increase in the groove width along the laser polarization direction, and an increase in the groove length along the laser propagation direction. This observation suggests that the FIB pre-treatment locally enhanced the electric field, thereby intensifying the interaction between the laser and the substrate. Moreover, at the location indicated by yellow arrow in Figure 9, periodic structures became evident after 125 pulses. These structures persisted even after 250 pulses and were observed only around FIB marks. This result indicates that the FIB marks likely acted as nucleation sites for LIPSS formation. In this study, the formation process of LIPSS was elucidated through *in-situ* SEM observation of the surface immediately after laser irradiation. Notably, Kodama *et al*. [18] demonstrated that the position and shape of LIPSS can be controlled by ultraprecision cutting, supporting the importance of surface structure in LIPSS formation.

In Fig. 7, the electric field enhancement around the FIB mark after 125-pulse irradiation is discussed with reference to the study by Shimizu *et al.* [19]. In their work, FDTD simulations showed that elliptical nanovoids with a length of ~200 nm and depth of 25–50 nm produces local electric field enhancement up to a factor of 5 at the tips aligned perpendicular to the laser polarization. In this study, the FIB marks were significantly larger (1 μm wide, 6 μm long, and 1 μm deep) and therefore had much lower curvature overall. As such, strong field concentration like that reported in [19] is not expected across the entire structure. However, nanoscale steps or roughness may remain at the edges of the FIB marks due to the milling process, potentially acting as localized field enhancers. As shown in Fig. 7, LIPSS formed preferentially in the vicinity of the FIB mark under 125-pulse irradiation. Since the formation of LIPSS generally requires localized enhancement of the electric field, this selective formation is considered indirect experimental evidence of field enhancement caused by the FIB-marked structure.

The above observation aligns with findings by Miyaji *et al.* [20], who demonstrated that nanostructure formation on submicron-striped surfaces—such as diamond-like carbon (DLC) and titanium nitride (TiN) films—can be initiated at points of high surface curvature, even at fluences below the single-pulse ablation threshold. In their study, periodic structures appeared first at the ridge tops in DLC and later expanded to flat regions, highlighting the critical role of initial topography in lowering the effective ablation threshold. Similarly, in conductive TiN films, high free-electron density caused localized field enhancement at the stripe edges. Consistent with these results, our study shows that even minimal surface modification by FIB can promote laser–material interaction via electric field enhancement, leading to groove widening and LIPSS formation in adjacent areas.

These findings reinforce the concept that local surface geometry strongly affects both the initiation and spatial distribution of LIPSS. Intentional introduction of surface scratches or patterns could therefore serve as a viable strategy for controlling the onset and characteristics of periodic structure formation.

4. Conclusion

In this study, we investigated the relationship between accumulated femtosecond laser pulses and the resulting periodic structures formed on Si and SiC surfaces. To enable *in-situ* observation of morphological changes, an *in-situ* observation system was developed by integrating an optical window into a SEM. This system allowed pulse-by-pulse monitoring of LIPSS evolution under identical irradiation conditions.

SEM observations revealed distinct differences between the two materials. On Si, periodic structures initially appeared as elliptical features and progressively expanded with increasing pulse number, suggesting the involvement of a positive feedback mechanism driven by local electric field enhancement. In contrast, SiC exhibited linear LIPSS that remained morphologically stable and evolved into branched patterns, with little dependence on the number of accumu-

lated pulses. This difference is attributed to the intrinsic thermal and optical properties of SiC, which suppress feedback-driven structural evolution.

Moreover, FIB pretreatment on Si surfaces led to the formation of periodic structures, indicating that surface morphology plays a key role in enhancing local electric fields and promoting LIPSS formation. These results suggest that controlled surface modifications—such as intentional scratches or nano-patterning—could serve as a strategy for initiating or guiding periodic structure formation in laser processing applications.

Acknowledgments

This work was partially supported by THE AMADA FOUNDATION (AF-2020201-A3), the Amano Institute of Technology, Power Academy, Iketani Science and Technology Foundation, and Nippon Sheet Glass Foundation for Materials Science and Engineering.

References

[1] M. Birnbaum: J. Appl. Phys., 36, (1965) 3688.
[2] J. Bonse, H. Sturm, D. Schmidt, and W. Kautek: Appl. Phys. A., 71, (2000) 657.
[3] F. Costache, M. Henyk, and J. Reif: Appl. Surf. Sci., 186, (2002) 352.
[4] N. Yasumaru, K. Miyazaki, and J. Kiuchi: Appl. Phys. A., 76, (2003) 983.
[5] A. Borowiec and H. K. Haugen: Appl. Phys. Lett., 82, (2003) 4462.
[6] J. Bonse, J. Krüger, S. Höhm, and A. Rosenfeld: J. Laser Appl., 24, (2012) 042006.
[7] R. Miyagawa, T. Ohgai, S. Yoshikawa, Hwan Hong Lim, S. Rezvani, T. Taira, and O. Eryu: Opt. Express., 32, (2024) 11863.
[8] K. Sokolowski-Tinten, J. Bailkowski, A. Cavalleri, D. von der Linde, A. Oparin, J. Meyer-ter-Vehn, and S. I. Anisimov: Phys. Rev. Lett., 81, (1998) 224.
[9] D. von der Linde and K. Sokolowski-Tinen: Appl. Surf. Sci., 154, (2000) 1.
[10] T. Suemoto, K. Terakawa, Y. Ochi, T. Tomita, M. Yamamoto, N. Hasegawa, M. Deki, Y. Minami, and T. Kawachi: Opt. Express., 18, (2010) 14114.
[11] T. Tomita, M. Yamamoto, N. Hasegawa, K. Terakawa, Y. Minami, M. Nishikino, M. Ishino, T. Kaihori, Y. Ochi, T. Kawachi, M. Yamagiwa, and T. Suemoto: Opt. Express., 20, (2012) 29329.
[12] T. Tomita, K. Kinoshita, S. Matsuo, and S. Hashimoto: Appl. Phys. Lett., 90, (2007) 153115.
[13] J. M. Liu: Opt. Lett., 7, (1982) 196.
[14] J. Bonse, S. Baudach, J. Krüger, W. Kautek and M. Lenzner: Appl. Phys. A, 74, (2002) 19.
[15] Laura Gemini, Masaki Hashida, Masahiro Shimizu, Yasuhiro Miyasaka, Shunsuke Inouem, Shigeki Tokita, Jiri Limpouch, Tomas Mocek, Shuji Sakabe: J. Appl. Phys., 114, (2013) 194903.
[16] Yasuhiro Miyasaka, Masaki Hashida, Takaya Nishii, Shunsuke Inoue, Shuji Sakabe: Appl. Phys. Lett., 106, (2015) 013101.
[17] S. A. Maier: “Plasmonics: Fundamentals and Applications”, (Springer, UK, 2007) p.27.
[18] Shuhei Kodama, Shinya Suzuki, Kazuya Hayashibe, Keita Shimada, Masayoshi Mizutani, Tsunemoto Kuriyagawa: Precis Eng, 55, (2019) 433.
[19] Masahiro Shimizu, Masaki Hashida, Yasuhiro Miyasaka, Shigeki Tokita, Shuji Sakabe: Appl. Phys. Lett., 103, (2013) 174106.
[20] G. Miyaji, Y. Miyatani, and K. Miyazaki: Rev. Laser Eng., 36, (2008) 1210.

(Received: June 5, 2025, Accepted: August 31, 2025)